Biomaterials 131 (2017) 131–144

Contents lists available at ScienceDirect

Biomaterials

journal homepage: www.elsevier.com/locate/biomaterials

Myofibroblastic activation of valvular interstitial cells is modulated by spatial variations in matrix elasticity and its organization

Hao Ma [a, b, 1], Anouk R. Killaars [b, c, 1], Frank W. DelRio [d], Chun Yang [b, e, 2], Kristi S. Anseth [a, b, f, *]

[a] Department of Chemical and Biological Engineering, University of Colorado at Boulder, Boulder, CO 80309, USA
[b] BioFrontiers Institute, University of Colorado at Boulder, Boulder, CO 80309, USA
[c] Department of Materials Science and Engineering, University of Colorado at Boulder, Boulder, CO 80309, USA
[d] Material Measurement Laboratory, National Institute of Standards and Technology, Boulder, CO 80305, USA
[e] Department of Chemistry and Biochemistry, University of Colorado at Boulder, Boulder, CO 80309, USA
[f] Howard Hughes Medical Institute, University of Colorado at Boulder, Boulder, CO 80309, USA

ARTICLE INFO

Article history:
Received 22 March 2017
Accepted 24 March 2017
Available online 28 March 2017

Keywords:
Hydrogels
Photopatterning
Matrix elasticity
Valvular interstitial cell (VIC)
α-smooth muscle actin (α-SMA)
Yes-associated protein (YAP)

ABSTRACT

Valvular interstitial cells (VICs) are key regulators of the heart valve's extracellular matrix (ECM), and upon tissue damage, quiescent VIC fibroblasts become activated to myofibroblasts. As the behavior of VICs during disease progression and wound healing is different compared to healthy tissue, we hypothesized that the organization of the matrix mechanics, which results from depositing of collagen fibers, would affect VIC phenotypic transition. Specifically, we investigated how the subcellular organization of ECM mechanical properties affects subcellular localization of Yes-associated protein (YAP), an early marker of mechanotransduction, and α-smooth muscle actin (α-SMA), a myofibroblast marker, in VICs. Photo-tunable hydrogels were used to generate substrates with different moduli and to create organized and disorganized patterns of varying elastic moduli. When porcine VICs were cultured on these matrices, YAP and α-SMA activation were significantly increased on substrates with higher elastic modulus or a higher percentage of stiff regions. Moreover, VICs cultured on substrates with a spatially disorganized elasticity had smaller focal adhesions, less nuclear localized YAP, less α-SMA organization into stress fibers and higher proliferation compared to those cultured on substrates with a regular mechanical organization. Collectively, these results suggest that disorganized spatial variations in mechanics that appear during wound healing and fibrotic disease progression may influence the maintenance of the VIC fibroblast phenotype, causing more proliferation, ECM remodeling and matrix deposition.

1. Introduction

Valvular interstitial cells (VICs), the most abundant cell type in heart valve tissue, actively regulate the structure and composition of the extracellular matrix (ECM) during wound healing and disease progression [1,2]. VICs fulfill their functional role in ECM remodeling by transitioning from a quiescent fibroblast phenotype to an activated myofibroblast phenotype with more contractility, higher matrix metalloproteinase (MMP) activity and more collagen production [2–5].

Under normal physiological conditions, the ECM that VICs synthesize and reside in has a highly organized distribution of collagen fibers [6], but during disease progression and wound healing, the organization of the collagen fibers that are newly synthesized by VICs is disturbed and alignment is lost [7]. Deposition of more collagen fibers results in a higher stiffness of the ECM, and the disorganization of new deposited collagen fibers leads to spatial variation of matrix mechanics [8,9]. *In vivo* studies showed that disorganized collagen deposition is a common phenomenon in different types of tissue. As one specific example, the group of Scully demonstrated that during valve fibrosis and heart disease

* Corresponding author. Department of Chemical and Biological Engineering, University of Colorado at Boulder, Boulder, CO 80309, USA.
E-mail address: kristi.anseth@colorado.edu (K.S. Anseth).
[1] These authors contributed equally to this work.
[2] Present Address: Department of Chemical and Biomolecular Engineering, University of California, Berkeley, CA, 94720, USA.

http://dx.doi.org/10.1016/j.biomaterials.2017.03.040
0142-9612/

progression with age, collagen fibers in human aortic heart valves become disorganized and lose alignment [7]. Collagen organization has also been studied during wound healing processes. Doillon and co-workers observed that the collagen distribution was poorly organized during wound healing in a full thickness defect in rat skin [10]. Furthermore, the group of Bodi showed that in swine, and more importantly in human, the collagen organization at the outer region of the myocardial infarcted area was more disorganized and random compared to the core region [11]. Other mechanical properties that changed during valvular ECM remodeling have been shown to affect VIC phenotypic change and functions, for example stress relaxation [12] and transvalvular pressure [13]. For this manuscript, we are specifically interested in the effect of randomized stiffness organization, which results from new deposited collagen fibers on VIC phenotypic change.

The observations of disorganized collagen distributions *in vivo* for fibroblast-rich regions also corresponded with findings from *in vitro* studies with VICs using a scratch wound model. At the edge of the wound, VICs were found to be more proliferative and to form more α-smooth muscle actin (α-SMA) fibers compared to VICs distal from the wound's edge [14]. Based on the different behavior of VICs as a function of their matrix environment and organization, the question arose if it was the organization of the ECM or the change in overall stiffness of the local microenvironment that affected VIC proliferation and phenotypic transition during disease progression and wound healing. We hypothesized that local variations in matrix mechanics (e.g., from organized to disorganized) would influence the phenotypic properties of VICs through a mechanotransduction process [15].

To test this hypothesis, we used a synthetic hydrogel platform with photo-tunable mechanical properties that allows us to spatially vary the matrix mechanics, as the nitrobenzyl groups in our hydrogel platform enable spatial control over the crosslinking density [15–17]. Photomasks with different lithographic patterns were used to fabricate hydrogels with patterned mechanical properties, both organized and disorganized, through photodegradation. Subsequently, porcine VICs, which similarly to other sources of fibroblasts, can undergo a fibroblast-to-myofibroblast transition, were cultured on these hydrogel substrates and VIC activation was characterized by the appearance of organized α-SMA stress fibers, a key myofibroblast marker [2,18–21]. During the transition into myofibroblasts, VICs form α-SMA stress fibers in the cytoplasm (α-SMA activated cells or activated VICs), while a diffuse α-SMA expression in the cytoplasm (α-SMA deactivated cells or deactivated VICs) has been observed for quiescent fibroblasts [2,20,21].

Yes-associated protein (YAP), a transcriptional co-activator that shuttles from the cytoplasm to the nucleus (YAP activation), is an indicator for cell mechanotransduction [22]. The foundation and majority of studies about YAP as a mechanotransduction indicator have been completed using mesenchymal stem cells as a model [23,24], but some recent studies with myofibroblasts have also shown that YAP activation is involved during the transition from fibroblasts into myofibroblasts [25–27]. However, our knowledge about how YAP is involved in the mechanotransduction process for VICs is still limited, especially the relationship and temporal order between the intracellular localization of YAP and α-SMA activation. Therefore, studies were conducted to investigate the relationship between YAP and α-SMA activation as a function of time and how mechanotransduction affects the VICs phenotypic transition. Ultimately, these studies provide insight into the impact of the organization of matrix mechanics on a wide range of VIC functions, as well as the role of mechanotransduction through YAP signaling on the VIC phenotypic transition.

2. Materials and methods

2.1. Synthesis of photo-degradable hydrogel components

Poly(ethylene glycol) di-photodegradable acrylate (PEGdiPDA) was synthesized and characterized as previously described [13,14]. Briefly, 4-[4-(1-acrylethyl)-2-methoxy-5-nitrophenoxy]butanoic acid (8 eq.) and poly(ethylene glycol) bis-amine (M_n ~ 3400 Da; Laysan Bio Inc.) (1 eq.) were dissolved in *N*-Methyl-2-pyrrolidone (NMP) (156 mmol). (1-[bis (dimethylamino)methylene]-1H-1,2,3-triazolo [4,5-b]pyridinium 3-oxid hexafluorophosphate) (HBTU) (9 eq.) and 1-hydroxybenzotriazole (HOBt) (9 eq.) were added and allowed to react over night. The product was precipitated in ice-cold diethyl ether and dialyzed against water (SpectraPor 7, MWCO 2000 Da; Spectrum Labs). Purity and conjugation was confirmed by ^{1}H NMR (~90% conjugation). The adhesive peptide, OOGRGDSG (diethylene glycol-diethylene glycol-glycine-arginine-glycine-aspartic acid-serine-glycine), was synthesized on a Tribute peptide synthesizer (Protein Technologies) using standard Fmoc solid phase peptide synthesis protocols [15]. The N-terminal amine was coupled with acrylic acid using HATU conditions on resin to yield the Acryl-OOGRGDSG monomer (acrylated RGD) [15]. The peptide was cleaved from the resin in 1 h (95% TFA, 2.5% triisopropylsilane (TIPS) and 2.5% DI H_2O). This mixture was precipitated in ether and centrifuged. The peptide was washed with ether and centrifuged two additional times and then dried under vacuum. Peptide purification was conducted using semi-preparative reversed-phase high performance liquid chromatography (RP-HPLC; Waters 2767, 2489, 2545) with a gradient of 5:95 acetonitrile:water with 0.1% (vol/vol) TFA over 70 min at 20 mL/min on a C18 5 μm preparation column. The purity of peptides was confirmed by matrix-assisted laser desorption-ionization time-of-flight mass spectrometry using α-cyano-4-hydroxycinnamic acid as a matrix. (MALDI-TOF MS, Applied Biosystems DE Voyage) as previously described in Ref. [15].

2.2. Photo-degradable hydrogel formulations

Photo-degradable hydrogels were polymerized as described previously [15]. Briefly, PEGdiPDA was copolymerized with PEG monoacrylate, M_n ~400 Da (PEG400A) (Monomer-Polymer and Dajac Laboratories, Inc.) and acrylated RGD through a redox-initiated free radical polymerization in PBS. Gel solutions were prepared with 5.25 wt% PEGdiPDA, 7.25 wt% PEG400A, 2.5 mM acrylated RGD and 200 mM ammonium persulfate (APS). A final concentration of 100 mM tetramethylethylenediamine (TEMED) was added to initiate the polymerization. Gels were formed in 6 min on acrylated cover glass with a 12 mm diameter.

2.3. Rheological characterization of bulk hydrogel properties

The dynamic moduli of hydrogels both before and during photodegradation were measured on a Discovery Hybrid Rheometer (TA Instruments) at room temperature. Optically thin hydrogels with a thickness of 100 μm were formed *in situ* between a Quartz bottom plate and an 8 mm diameter stainless steel upper plate. The gel network evolution was monitored using a dynamic time sweep at 1% strain and an angular frequency of 3 rad/s. After the storage modulus (G') reached its plateau at 3.37 ± 0.02 kPa, degradation was started by collimated 365 nm light ($I_0 = 10$ mW/cm^2; Omnicure 1000, Lumen Dynamics), and the change in G' was monitored using the same dynamic time sweep parameters until the G' reached 1.93 ± 0.17 kPa, 1.31 ± 0.02 kPa and 0.69 ± 0.03 kPa, respectively. Young's modulus was calculated with $E = 2 * (1 + \nu) * G'$, where a Poisson's ratio (ν) of 0.5 for the PEG hydrogels was assumed [28].

This led to Young's moduli around 10, 6, 4 and 2 kPa. Young's modulus will be reported to indicate the modulus of the hydrogels for all subsequent discussions.

2.4. Photopatterning to generate hydrogels with spatially varying mechanical properties

Hydrogels with spatially varying moduli were fabricated by controlled illumination using chrome photo-masks (Photoscience Inc.). For all experiments, initial hydrogel formulations had a Young's modulus (E) of 10 kPa. Thus, unexposed regions remained at 10 kPa, while the exposed areas underwent photodegradation to reduce the local modulus. These regions were exposed to collimated 365 nm light for 400 s ($I_0 = 10$ mW/cm^2; Omnicure 1000, Lumen Dynamics), which led to a reduction in E to 4 kPa. A series of masks with regularly and randomly spaced squares allowed for controlled illumination of the underlying hydrogel substrate. Each patterned region was 2 μm by 2 μm which is similar in size with a mature focal adhesion [15]. The repeat unit of the regular and random pattern was 50 μm by 50 μm, so that each individual VIC sensed the same stiffness organization on the same substrate. The masks were selected to allow for 0, 25, 50, 75, 89, or 100% of light transmission, which then yielded hydrogels with both "stiff" (10 kPa) and "soft" (4 kPa) regions at a stiff-to-soft ratio of 100:0, 75:25, 50:50, 25:75, 11:89, and 0:100.

2.5. Atomic force microscopy characterization of spatially varying hydrogel properties

Atomic force microscopy (MFP-3D Classic, Asylum Research) was used to measure the spatially varying elastic moduli of the patterned PEGdiPDA hydrogels. Briefly, force-spectroscopy was performed at each point in a 64 × 64 square grid over a 10 μm × 10 μm area, resulting in "force-volume" modulus maps for hydrogels with regular and randomized patterns. The measurements were conducted in deionized water at room temperature using the fluid cell lite assembly for the MFP-3D Classic. Triangular SiN cantilevers with sharp Si tips (Bruker SNL-10 cantilevers with a nominal radius $R \approx 2$ nm) were used to minimize the interaction volume between measurements. Each probe was calibrated using the thermal fluctuation method [29] and imaged via scanning electron microscopy (SEM); the resulting values for the spring constant of the probe k_c varied from 0.09 N/m to 0.16 N/m and the half-angle of the tip α varied from 18° to 24°. AFM force-displacement (*F-d*) data were acquired as the probe tip was loaded and unloaded from the hydrogel surface. The maximum force was 5 nN, and the displacement rate during loading and unloading was constant at 10 μm/s. *F-d* curves were converted to force-deformation (*F*-δ) data by subtracting cantilever deflection. The loading portion of each *F*-δ data set was fit to an analytical model for a rigid conical tip in contact with an elastic half-space [30] to find Young's modulus *E*, using an average value for α from SEM, an assumed Poisson's ratio for the hydrogel ($\nu = 0.5$), and *E* as the sole fitting parameter. The height difference between the stiff and soft regions is slightly larger than that depicted in AFM images given the difference in moduli between the two regions.

2.6. Valvular interstitial cell isolation and culture

Valvular interstitial cells (VICs) were isolated from fresh porcine hearts (Hormel) as previously described [31]. Briefly, porcine aortic valve leaflets were excised from the hearts, rinsed in Earle's Balanced Salt Solution (Life Technologies) with 1% penicillin-streptomycin (Life Technologies) and 0.5 mg/mL fungizone (Life Technologies) and subsequently incubated in a collagenase solution (250 units/mL, Worthington) for 30 min at 37 °C. Endothelial cells were removed by vortexing and centrifugation, followed by another incubation in collagenase solution for 60 min at 37 °C. Filtration of the solution with a 100 μm cell strainer was conducted to separate VICs from the remaining extracellular matrix. Next, VICs were pelleted by centrifugation and then re-suspended in growth media, Media 199 (DMEM, Gibco Life Technology #11150-059) supplemented with 15% fetal bovine serum (FBS, Life Technologies), 2% penicillin-streptomycin, and 0.5 mg/mL fungizone. The isolated VICs were expanded on tissue culture polystyrene (TCPS) until 80% confluence and frozen down in FBS containing 20% DMSO and stored in liquid nitrogen as Passage 1 (P1). P2 to P4 VICs were generated by expanding the P1 stock in growth media (DMEM supplemented with 15% FBS, 50 U/ml penicillin, 50 mg/mL streptomycin and 1 mg/mL fungizone), and P2 to P4 VICs were used in all the reported experiments. VICs were cultured on TCPS in growth media at 5 × 10^5 cells/cm^2 for two days prior to seeding on hydrogels at 10,000 cells/cm^2 in media with a serum level of 1% FBS. 1% FBS was selected to reduce proliferation and minimize differences in cell density across the hydrogel conditions. Hydrogel samples were then transferred to a new plate with fresh media 24 h post cell seeding to eliminate any confounding influence of VICs that attached to the TCPS instead of the hydrogels. Samples were fixed 24, 72 or 120 h after cell seeding. In order to provide sufficient time for cell attachment and spreading on the substrates from suspension in the medium, 24 h was chosen as the first time point for focal adhesion and YAP activation analyses.

2.7. Immunostaining

VICs were fixed in 4% paraformaldehyde for 45 min at room temperature, rinsed in PBS twice, and then permeabilized using 0.1% TritonX-100 in PBS for 1 h. Next, samples were blocked in 5% bovine serum albumin (BSA) overnight at 4 °C to minimize non-specific protein binding. Anti-YAP (1:250, mouse, Santa Cruz) and anti-αSMA (1:200, rabbit, Invitrogen) primary antibodies in 5% BSA were applied to samples and incubated for 1 h at room temperature. Anti-paxillin (1:400, mouse, Thermofisher scientific) primary antibody in 5% BSA was applied to samples and incubated over night at 4 °C. Primary antibodies were removed by rinsing in PBST (0.5 wt% Tween-20 in PBS) two times for 10 min. Samples were then incubated at room temperature with secondary antibodies (1:1000, goat anti-rabbit AlexaFluor 488; goat anti-mouse AlexaFluor 647, invitrogen), phalloidin (1:1000, Sigma Aldrich) and DAPI (1 mg/mL; Sigma) in 1% BSA. After 1 h, the secondary antibody solution was removed and the samples were rinsed three times for 10 min with PBST. All immunostained samples were stored in PBS at 4 °C until imaging (Operetta; Perkin Elmer). Although transcriptional coactivator with PDZ-binding motif (TAZ) has been identified as an important mechanotransducer in fibroblasts besides YAP, only staining with YAP was performed in this study as TAZ is paralog of YAP and they are always colocalized with each other when being activated and deactivated.

2.8. RNA isolation and quantitative real-time polymerase chain reaction

Quantitative real-time polymerase chain reaction (qRT-PCR) was used to quantify the mRNA expression levels of α-SMA and Collagen 1A1 (COL1A1) relative to the reference gene for ribosomal protein L30. RNA was isolated from VICs on 3 substrates (A ~1520 μm^2) 72 h after seeding onto the hydrogels by using TriReagent (SigmaAldrich) following manufacturer's instructions. RNA was precipitated by 2-propanol (SigmaAldrich) and RNA pellets were washed twice with 75% ethanol. After re-suspension of the

pellets in water, RNA quantity and purity was measured via spectrophotometry (ND-1000; NanoDrop). cDNA was synthesized from total RNA using the iScript Synthesis kit (Bio-Rad). Relative mRNA expression levels were measured via qRT-PCR using SYBR Green reagents (Bio-Rad) on an iCycler (Bio-Rad) and normalized to a reference gene, ribosomal protein L30, in experimental samples. Three technical replicates were performed for each biological replicate. Primer sequences are listed in Table 1.

2.9. VIC proliferation

The proliferation of VICs as a function of hydrogel substrate stiffness organization was monitored in both 1% and 15% FBS, corresponding to conditions for low and high levels of VIC proliferation. To quantify proliferation, 10 μM EdU in PBS (ThermoFisher, Cat# C10340) was added to the culture at 36 h and allowed to incubate for another 36 h before fixation. The samples were subsequently rinsed in 3% BSA twice, followed by permeabilization in 0.1% TritonX-100 in PBS for 1 h. After rinsing with 3% BSA, samples were incubated with the Click-iT reaction cocktail prepared from the Click-iT EdU Alexa Fluor 647 kit (ThermoFisher, Cat# C10340) for 30 min at room temperature. Samples were washed once with 3% BSA and once with PBS. After this, immunostaining was continued as described before. Mitomycin C (Sigma-Aldrich, Cat# M4287) was added at a concentration of 10 μg/mL 24 h after seeding during the proliferation inhibition experiments. After incubation with Mitomycin C for 2 h, two 1 h washes with 1% FBS medium without Mitomycin C were performed to wash away the excess Mitomycin C.

2.10. VIC-hydrogel interactions: morphology, focal adhesions, proliferation and activation

Morphology and activation were analyzed using Harmony High Content Imaging and Analysis software (Perkin Elmer). This software has been widely applied for acquisition and quantitative analyses of fluorescent immunostaining images [32]. For nucleus and cell morphology, nuclear and cytoplasmic outlines were identified based on DAPI and F-actin staining, respectively, using the Find Nuclei and Find Cytoplasm building block. The area and roundness were quantified by using the Calculate Morphology Properties building block. YAP activation was quantified by first measuring the mean intensity of the YAP staining in the nucleus area and cytoplasm area using the Calculate Intensity Properties building block. In the Define Results building block, cells with a 1.7 times higher YAP intensity were classified as YAP activated cells. The threshold of 1.7 was chosen based on the scatterplot of the ratio between the YAP intensity in the nucleus and the YAP intensity in the cytoplasm. This also matched with manual counting. α-SMA activation was counted manually based on stress fiber formation in the cytoplasm. VICs with α-SMA stress fiber formation were classified as α-SMA activated cells. The focal adhesion area was measured with ImageJ. The background was subtracted using a rolling ball radius of 10 pixels. The image was thresholded, made binary, and the area was calculated by the Analyze Particles function. During the analyses, large cell clusters were avoided and only single isolated cells and cells that barely touch boundary were analyzed.

Table 1
Primer sequences for qRT-PCR.

Gene	Forward primer (5′-3′)	Reverse primer (5′-3′)
L30	GCTGGGGTACAAGCAGAC	AGATTTCCTCAAGGCTGG
α−SMA	GCAAACAGGAATACGATGAAGCC	AACACATAGGTAACGAGTCAGAGC
COL1A1	GGGCAAGACAGTGATTGAATACA	GGATGGAGGAGTTTACAGGAA

2.11. Statistical analysis

For each experiment, at least 3 biological replicates were performed using different pools of porcine hearts with 3 technical replicates in each biological replicate. Each pool of porcine VICs consists of at least 10 porcine hearts. For morphology, proliferation and activation analyses, at least 200 cells were analyzed per condition per technical replicate. For focal adhesions, at least 20 cells were analyzed per technical replicate. Data were compared using one-way ANOVAs and Bonferroni post-tests in Prism 7 (GraphPad Software, Inc) unless otherwise stated. Data is presented as mean ± standard error.

3. Results

3.1. VICs sense matrix mechanics within a narrow range

The VIC fibroblast-to-myofibroblast transition is known to depend on the chemistry and mechanics of the VIC's surrounding microenvironment [20,33–37]. Here, we were particularly interested in VIC mechanosensing and the role of extracellular matrix mechanics and its organization on VIC activation. For these experiments, VIC myofibroblast activation was characterized by α-SMA fiber formation and mechanosensing through nuclear localization of the transcription co-activator YAP. To control the VIC microenvironment, hydrogels with tunable material properties were synthesized by copolymerizing PEG monoacrylate (PEG400A) molecules with PEG diacrylate (PEGdiPDA) crosslinkers, containing photodegradable nitrobenzyl ether groups [15,17] (Fig. 1A). The formulation also included an acrylated-RGD adhesive peptide sequence as a pendant functionality to promote VIC attachment to the PEG-based hydrogels. The PEGdiPDA crosslinker enables photocontrolled cleavage and control of the hydrogel crosslinking density, and subsequently the material modulus. Here, 365 nm light (intensity I_0 = 10 mW/cm^2) was used to soften the hydrogel system uniformly, but also in a spatially defined manner by controlled illumination.

First, hydrogel formulations with an initial storage modulus (G') of 3.37 ± 0.02 kPa and Young's modulus (E) of ~10 kPa were synthesized [28], and subsequently degraded by 10 mW/cm^2 of 365 nm light for 475 s, 400 s or 200 s. By controlling the light dose, hydrogels with varying G' were fabricated, ranging from 0.69 ± 0.03 kPa, 1.31 ± 0.02 kPa and 1.93 ± 0.17 kPa, which corresponded to E of ~2 kPa, 4 kPa and 6 kPa, respectively (Fig. 1B). The viscous modulus (G'') was consistently several orders of magnitude lower than the elastic modulus (G'), both before and after light exposure (Fig. 1C), so results primarily report on the elastic component of the modulus. From now on, E will be used to reference each hydrogel substrate. It is also important to note that for these degradation conditions and RGD concentrations, minimal changes (less than 5%) in the adhesive ligand density were observed upon photodegradation [15]. This is because the adhesive ligands are conjugated to the nondegradable kinetic chains, thus remained relatively unaffected during photodegradation.

Porcine VICs were cultured on PEG hydrogels with varying moduli for 72 h to allow establishment of mature matrix interactions and α-SMA stress fiber formation [26]. VICs on the stiffer substrates (6 kPa and 10 kPa) formed distinct α-SMA stress fibers compared to those cultured on the softer substrates (2 kPa and 4 kPa), where α-SMA was diffusely distributed throughout the cytoplasm based on immunostaining as shown by representative images in Fig. 2A. Specifically, the inset image of 4 kPa represented diffuse α-SMA, where no stress fiber can be found in the cytoplasm,

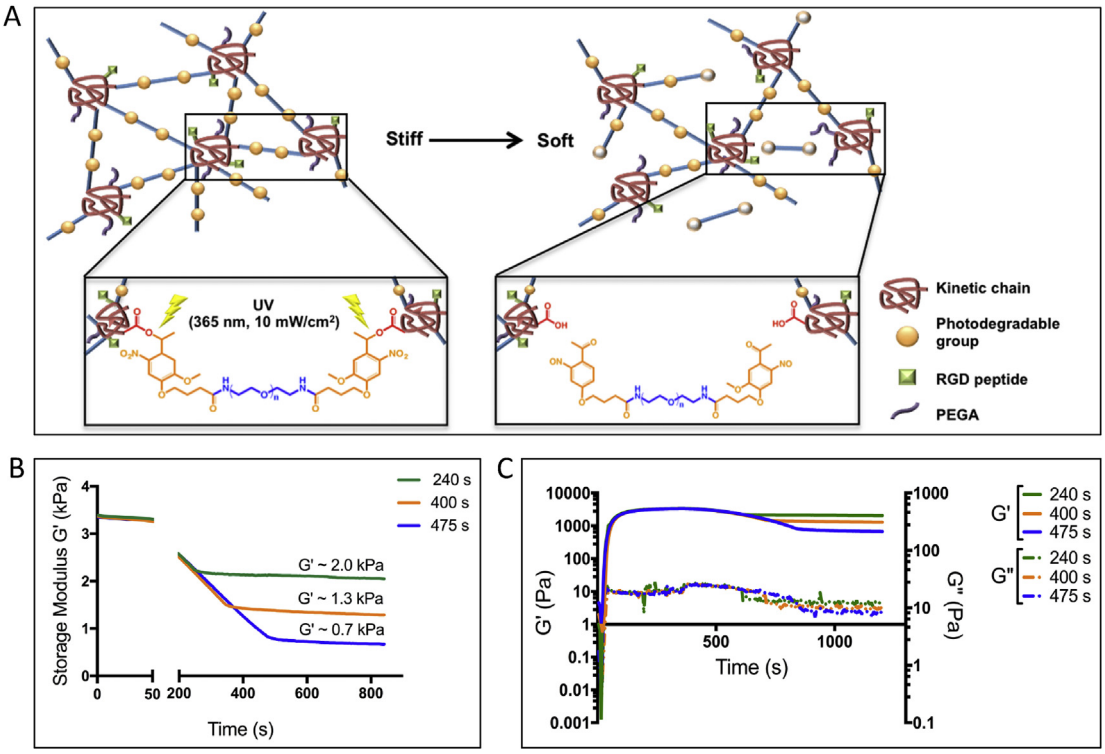

Fig. 1. VICs culture platform chemistry with degradation dynamics. A: Copolymerization of PEG400A and PEG with a photodegradable linker creates gels composed of poly(acrylate) kinetic chains (red coils) connected by PEG (blue lines with photodegradable groups (yellow solid sphere). Upon irradiation with UV light, the photodegradable groups were cleaved (yellow open sphere) and decreased the crosslinking density, therefore, a softer gel was created. **B**: Photodegradable hydrogels can be softened from a storage modulus of 3.37 ± 0.02 kPa to softer moduli of 1.93 ± 0.17 kPa, 1.31 ± 0.02 kPa and 0.69 ± 0.03 kPa by varying the UV irradiation time. **C**: The viscous modulus was measured to be consistently lower than elastic modulus before and after UV light exposure. (For interpretation of the references to colour in this figure legend, the reader is referred to the web version of this article.)

and the inset image of 10 kPa represented α-SMA stress fiber formation in the cytoplasm.

Additionally, YAP nuclear localization in VICs responded to substrate stiffness consistently with their myofibroblastic activation. Namely, on the stiffer substrates (6 and 10 kPa), YAP was found to be localized in the nuclei in more than 70% of the VIC population (73% for 6 kPa substrate and 76% for 10 kPa substrate). In contrast, only 50% and 40% of VICs were found to have nuclear YAP on 2 kPa and 4 kPa hydrogel substrates respectively (Fig. 2B(i)). This statistically significant difference in YAP localization was also shown by representative images in Fig. 2A, 10 kPa for nuclear-localized, activated YAP and 4 kPa for cytoplasmic-diffused, deactivated YAP. These results indicate that VICs are capable of perceiving a difference in the substrate moduli within a narrow range from 4 to 6 kPa based on YAP subcellular localization and α-SMA stress fibers formation.

Further investigation related to VIC morphology on these substrates was conducted to determine if VIC-matrix interactions (e.g., as measured by cell area and circularity) were significantly different over this moduli range. In particular, we aimed to avoid confounding effects in cellular signaling, as cell morphology has been previously reported to be an independent factor that can overwrite cell fate regardless of matrix mechanics [23,38]. Results show that VICs maintained similar morphologies, in both cell area and circularity, on the 4, 6 and 10 kPa substrates (Fig. 2B(ii)). However, VICs cultured on the 2 kPa substrate were significantly smaller and showed a more rounded morphology, which was statistically different compared to those on 4, 6 and 10 kPa substrates (Fig. 2B(ii)).

Moreover, cell nuclear shape has been previously studied as an important measure of mechanical sensing, and more specifically an indicator of cytoskeleton organization, cell morphology and differentiation of mesenchymal stem cell [39–42]. Thus, nuclear shape factors (area and circularity) were analyzed, and no significant differences were observed among VICs cultured on the 4, 6 and 10 kPa hydrogels (Supplemental Fig. 1). Importantly, a different nuclear morphology was only observed for VICs cultured on 2 kPa substrate, specifically a smaller nuclear area and higher circularity.

Based on these results, the 4 kPa and 10 kPa hydrogels were chosen as the soft, de-activating and stiff, activating substrates, respectively, to stimulate two different mechanosensing pathways in VICs and to study the effect of spatial organization of the matrix mechanics on VIC phenotypic changes. This narrow mechanics range has the same magnitude as physiologically relevant moduli [43] of the heart valve and minimized the change in chemical properties.

In order to confirm our conclusion that VICs can sense the moduli difference between 4 kPa and 10 kPa, mRNA expression levels of α-SMA and Collagen 1A1 were quantified by quantitative real-time polymerase chain reaction (qRT-PCR). As shown in Supplemental Fig. 2, mRNA expression levels of both genes were significantly up-regulated for VICs on stiff (10 kPa) substrates compared to VICs on soft (4 kPa) substrates, which is consistent with the α-SMA activation trend observed by immunostaining. Therefore, we strengthen our conclusion that VICs are capable of sensing the difference of moduli between 4 kPa and 10 kPa, independently of cell morphology.

3.2. Fabrication of spatially patterned hydrogel matrix mechanics

To understand how spatial variations in extracellular matrix mechanics might influence VIC mechanosensing and, ultimately,

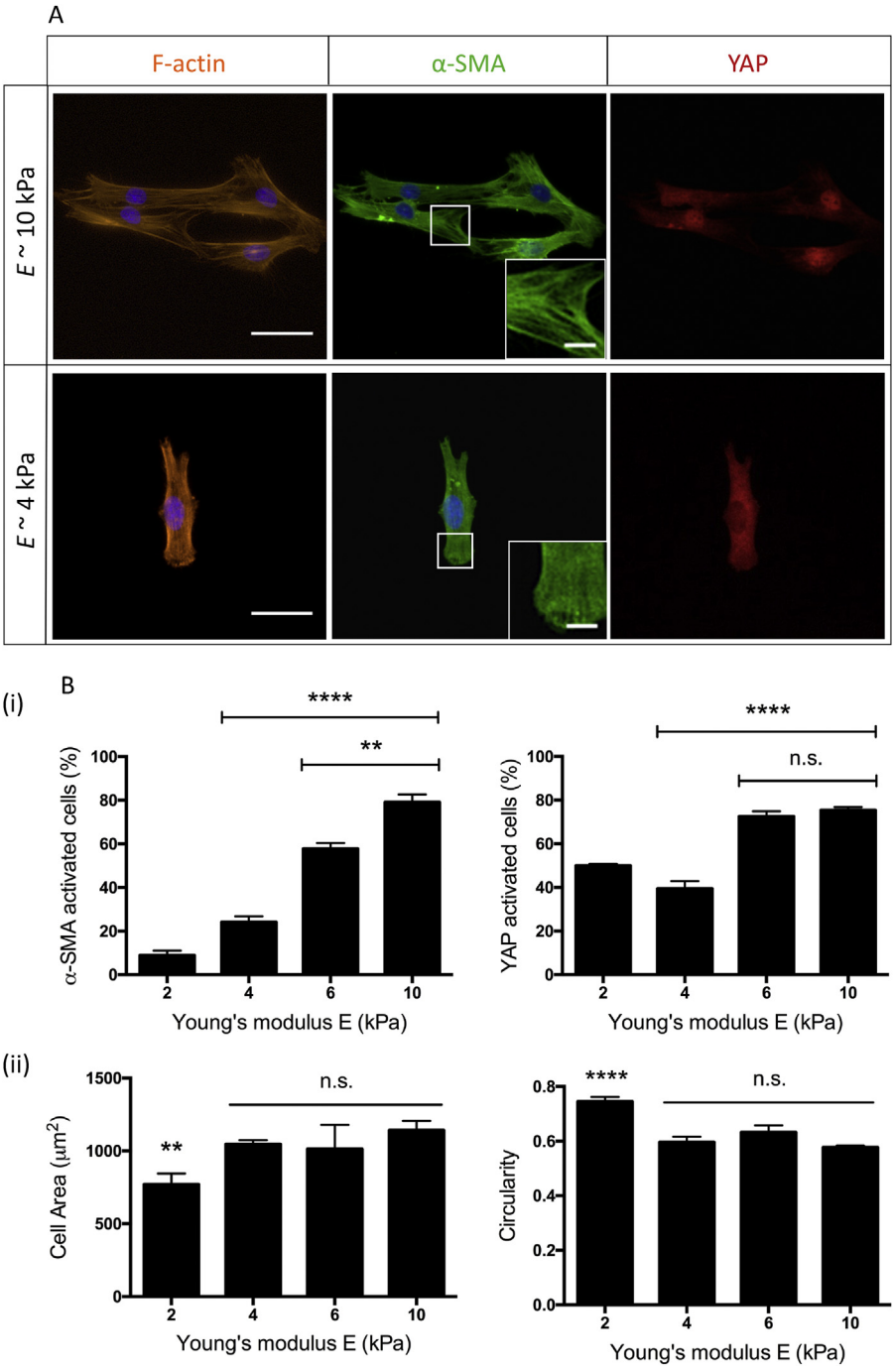

Fig. 2. Characterization of YAP and α-SMA activation on uniform substrates. A: Immunostaining of VICs on soft (4 kPa) and stiff (10 kPa) hydrogel surfaces after culturing for 72 h. On soft hydrogels, VICs have diffuse α-SMA expression in the cytoplasm with 24% α-SMA activation and 40% YAP activation, whereas on the stiff substrate, VICs showed α-SMA fiber formation with 79% α-SMA activation and 76% nuclear YAP activation. DAPI (blue), F-actin (orange), α-SMA (green), YAP (red). Scale bars = 50 μm. Inset image is magnification of outlined area, scale bar = 10 μm. **B: (i)**: The percentage of VICs expressing α-SMA fibers and nuclear localized YAP was quantified based on the immunostaining. Both the percentage of α-SMA activated and YAP activated cells increased when the gel modulus of their substrate was increased and there was found to be a high significant difference between 4 and 10 kPa substrates. ****: $p < 0.0001$. **: $p < 0.01$, based on one-way ANOVA analysis. n = 3 with triplicates, more than 200 VICs were analyzed per sample. **(ii)**: Cell morphology was analyzed by quantifying cell area and circularity based on the immunostaining. There was found to be no significant for both cell area and circularity, whereas there is a significant difference for the VICs on 2 kPa substrate. **: compared to 10 kPa, $p < 0.01$. ****: compared to 10 kPa, $p < 0.0001$, based on one-way ANOVA analysis. n = 3 with triplicates, more than 200 VICs were analyzed per sample. (For interpretation of the references to colour in this figure legend, the reader is referred to the web version of this article.)

their myofibroblast phenotype, PEG hydrogels with spatially varying mechanical properties were fabricated. Lithographic masks of 2 μm by 2 μm squares were used to create patterns of illuminated light, and based on exposure time and ratio of light to dark squares, patterns in mechanical properties across the hydrogel surface were introduced as shown in Fig. 3A. Regular patterns with different percentages of stiff, 10 kPa regions (11%, 25%, 50%, 75%) were created in the unexposed areas, while the exposed areas were the soft, 4 kPa regions (89%, 75%, 50%, 25%), correspondingly. Besides regular patterns with different percentages of stiff versus soft

regions, randomized patterns with the same ratio of stiff and soft regions were designed (Fig. 3A and Supplemental Fig. 3) [15]. More specifically, as shown in Supplemental Fig. 3, a 50 μm by 50 μm repeat unit was repeated throughout the substrate surface, in order to have each individual cell sense the same stiffness organization. The substrates with random patterns were selected to study the effect of heterogeneous versus organized variations in the extracellular matrix mechanical environment on VIC activation. Finally, uniformly 4 kPa (0% stiff region) and 10 kPa (100% stiff region) hydrogels were used as the soft and stiff controls.

To confirm the rheological measurements and to demonstrate the fidelity of the pattern transfer with exposure conditions, atomic force microscopy (AFM) was used to map the spatial variations in the hydrogel modulus. Representative images for the 75% and 11%

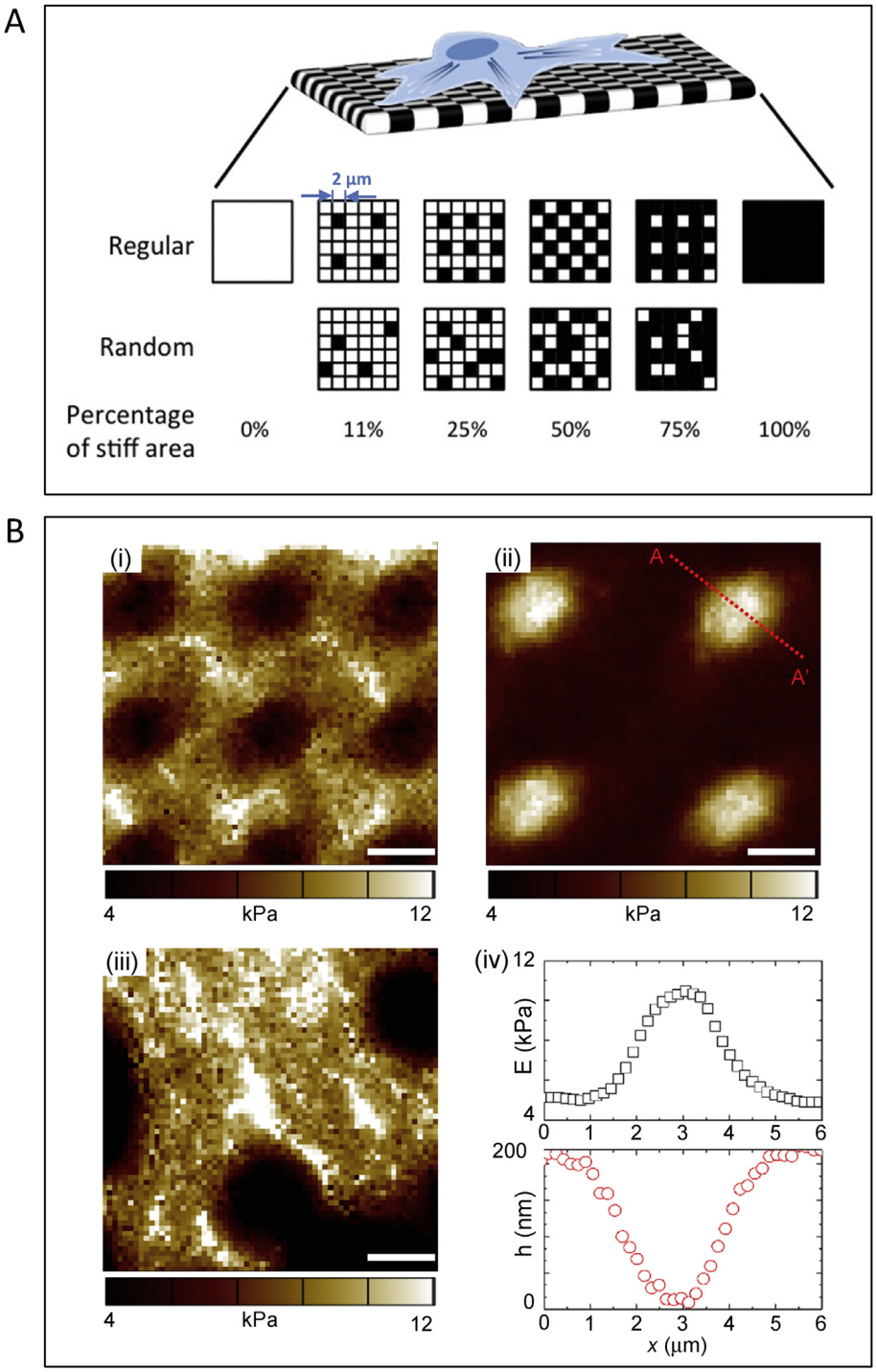

Fig. 3. Characterization of patterned substrates. A: An illustration of VICs seeded on hydrogel surfaces with different organizations of stiff regions (Modified from [15]). The percentages of stiff area is varied together with the organization (regular/random) of these areas. Black indicates areas that are covered with the photomask allowing them to retain the initial modulus of 10 kPa. The white squares indicate areas that are exposed to the UV light, resulting in degradation to 4 kPa. Each small square is 2 μm × 2 μm and each repeat unit is 50 μm × 50 μm. **B**: AFM elastic moduli maps of (i) 75% stiff (regular pattern), (ii) 11% stiff (regular pattern), and (iii) 75% stiff (random pattern) hydrogels. (iv) Elastic modulus E and surface height h as a function of position x for cross-section AA′ in (ii). Scale bars = 2 μm.

stiff regular patterns and the 75% stiff random pattern are shown in Fig. 3B (i), (ii), and (iii), respectively. As shown in the AFM measurements, the spatial variations in *E* correspond to the photomask lithographic patterns, indicating successful pattern transfer during the photodegradation process. In addition, it is evident from the cross-sectional data in Fig. 3B (iv) that the modulus data from the AFM measurements are in good agreement with data from the bulk rheological measurements, with the stiff and soft regions exhibiting *E* values ~10 kPa and ~4 kPa, respectively. The cross-sectional topography data from the same region in Fig. 3B (iv) also indicates that the photodegradation process resulted in spatial variations in mechanical properties with minimal changes in topography. At the stiff-to-soft boundary, the hydrogels exhibit a ~200 nm change in surface height based on AFM measurement, and hence maintain a constant adhesive area cross conditions of different stiff-to-soft ratios, as also demonstrated in previous work [15].

3.3. α-SMA and YAP activation in VICs depend on local variations in the matrix mechanics

To test the hypothesis that matrix mechanics influences VIC mechanotransduction and myofibroblastic activation in a manner that depends on the magnitude and organization of spatial stiffness, porcine VICs were cultured on hydrogel substrates with different percentages of stiff regions in both regular and random patterns. α-SMA and YAP activation was measured. First, no statistically significant differences were observed in the cell or nucleus morphology between any of the substrates (Supplemental Fig. 4). Moreover, VICs cultured on regularly-patterned substrates with a higher percentage of stiff regions exhibited more α-SMA stress fiber formation compared to VICs cultured on substrates with a higher percentage of soft regions, as shown by representative images in Fig. 4A. Namely, 34% and 82% of VICs were myofibroblasts on 11% and 75% stiff substrates, respectively. Hence, a positive correlation between α-SMA stress fibers formation and the percentage of stiff regions was observed.

Similarly, VICs cultured on hydrogel substrates with randomized patterns, showed statistically significant differences in α-SMA expression between substrates with a higher percentage of stiff regions and substrates with a higher percentage of soft region. Specifically, VICs on 11% random and 75% random substrates were 26% and 45% α-SMA positive, activated myofibroblasts (Fig. 4B). The trends of increasing α-SMA positive cells with increasing percentages of stiff regions for regularly- and randomly-patterned matrix mechanics variations support the notion that VICs sense variations in the local stiffness and that this results in changes in the key phenotypic marker.

Interestingly, a significant difference in the percentage of α-SMA stress fiber positive cells (i.e., myofibroblasts) was observed between the regular and random patterns, even with the same ratio of stiff to soft regions. For example, with 75% stiff regions, 82% versus 45% of VICs were myofibroblasts on regularly versus randomly patterned substrates, respectively (Fig. 4A and B). Thus, VICs not only respond in an integrated way to matrix mechanics, but the organization of the local matrix and its properties appear to play a role.

3.4. VICs proliferate more on matrices with random mechanical patterns

The stark differences between myofibroblast activation on regular versus random patterns led us towards experiments to characterize more directly whether VICs better maintain their quiescent fibroblastic phenotypes on substrates with disorganized modulus patterns. We hypothesized that the phenomenon might be related to the fact that VICs proliferate more at the early stages of disease development and wound healing processes, presumably to increase the cell population for further ECM remodeling and tissue deposition.

To test this hypothesis, VIC proliferation was measured after 72 h of culturing in medium with 1% FBS using EdU staining. Results are presented in Fig. 5, and a significant difference was observed in the percentage of VICs that were proliferating when cultured on the 75% regularly versus the 75% randomly patterned substrates. The 75% condition was selected based on the large differences observed in α-SMA activation between the regular and random patterns (Fig. 4). Consistent with previous characterization of VIC proliferation rates on hydrogels [44], the number of proliferating cells was relatively low, below 10%. This result is also consistent with the fact that medium with 1% FBS was used during the culture to maintain consistent cell densities on the substrates throughout the duration of the experiment [45]. However, when typical expansion medium was used (15% FBS) [46], more striking differences were observed between VIC proliferation on the 75% regular versus random patterned matrices. As shown in Fig. 5A and Supplemental Fig. 5, on the regular patterns, 32% of VICs were proliferating and recall that 78% of the cells were myofibroblasts. In contrast, on the randomly patterned materials, only 35% of the cells were myofibroblasts, but 54% of the VICs were proliferating.

We hypothesized that the differences observed in proliferation likely relate to the differences in VIC activation, so further analysis was completed to ascertain the percentage of proliferating VICs among the fibroblast versus myofibroblast populations. As shown in Fig. 5B, for both VICs on the 75% regular and random patterns, ~20% of the VIC myofibroblasts were proliferating compared to ~70% of the VIC fibroblasts. In other words, the VIC fibroblastic phenotype proliferates significantly more than the myofibroblastic phenotype and this phenomenon was also observed in studies about human dermal fibroblasts [47]. As the cytoskeleton and cell morphology are altered during cell division, it might be possible that a higher proliferation rate maintains the fibroblastic phenotype of VICs. To shed light on the causal relationship between proliferation and the phenotypic change, Mitomycin C was used to inhibit proliferation [48]. α-SMA activation was quantified after 72 h of culturing. As shown in Supplemental Fig. 4, proliferation was inhibited for VICs seeded on both 75% regular and 75% random patterns, while the differences of α-SMA activation between the two conditions remained. Hence, we proved that proliferation is a characteristic of the fibroblastic phenotype for VICs, instead of a causation of phenotypic change.

3.5. YAP nuclear localization positively correlates with α-SMA activation in VICs

As a transcriptional co-activator that also plays an important role in mechanotransduction processes for various cell types including VICs, YAP subcellular localization was used as a readout of mechanical signaling [22] and correlated to VIC myofibroblast activation [26,49]. We hypothesized that YAP activation in VICs would be affected by spatial variations in matrix mechanics. When VICs were cultured on substrates with a higher percentage of stiff areas, higher nuclear localization of YAP was observed (Fig. 6A). When the images were quantified, 33% of VICs showed nuclear localized YAP on the 11% regular and 64% on the 75% regular substrates. Fig. 6B plots the result for this analysis for all patterned substrates, and a trend of increasing YAP activation with higher levels of stiff regions in the substrate is observed. This trend is similar to that observed for α-SMA stress fibers. However, unexpectedly, there were no significant differences in YAP activation

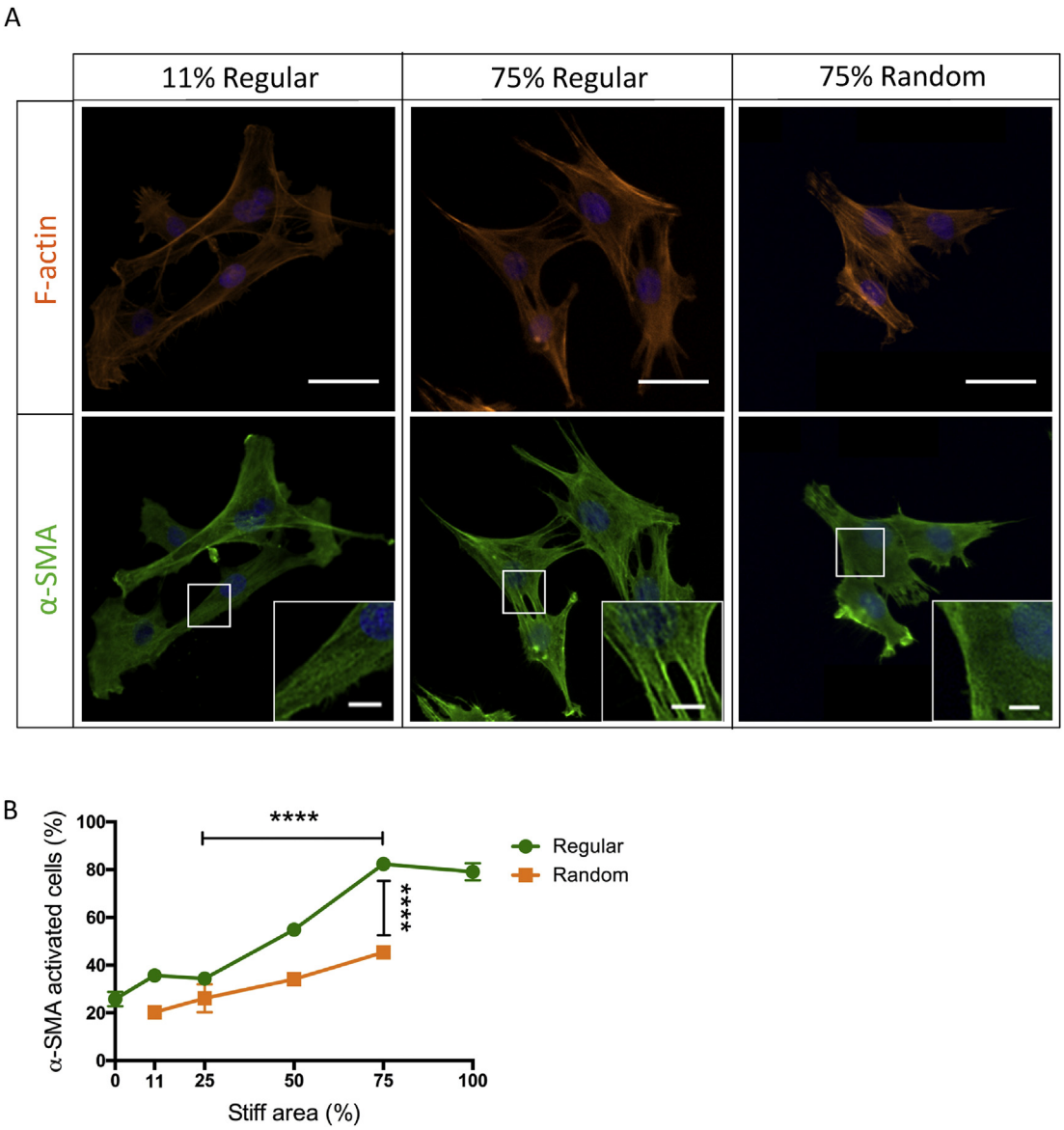

Fig. 4. Characterization of α-SMA activation on patterned substrates. A: Immunostaining of VICs on regular and random hydrogel surfaces after culturing in medium with 1% FBS for 72 h. F-actin fiber formation was seen on 11% and 75% regular and random substrates. α-SMA activation was only seen on the 75% regular substrate. DAPI (blue), F-actin (orange), α-SMA (green). Scale bars = 50 μm. Inset image is magnification of outlined area, scale bar = 10 μm. **B**: The percentage of VICs expressing α-SMA fibers was quantified based on the immunostaining. For regular patterns α-SMA activation increases correspondingly to stiff percentages. There was found to be a significant increase in α-SMA activation from 25% regular to 75% regular (green line with circles). However on random pattern this increase in α-SMA activation was not profound (orange line with squares), leading to a high significant difference between 75% regular and random substrates. ****: $p < 0.0001$, based on one-way ANOVA. n = 3 with triplicates, more than 200 VICs were analyzed per sample. (For interpretation of the references to colour in this figure legend, the reader is referred to the web version of this article.)

between regular and random patterns when compared at the same level of stiff region (Fig. 6B). Similar with α-SMA activation, YAP activation is independent of cell proliferation, as the YAP activation trend remained the same with inhibition of proliferation (Supplemental Fig. 6).

This result led us to investigate whether YAP and α-SMA activation have a temporally correlated relationship, as YAP has been reported as an early marker in the mechanotransduction cascade, while α-SMA is known as a more mature marker during the fibroblast-to-myofibroblast transition [26,49]. So further investigation of YAP and α-SMA activation was performed at different time points (24, 72 and 120 h) for VICs cultured on the 75% regular and 75% randomized patterned substrates. As shown in Fig. 7, an increase in both YAP activation levels and α-SMA activation levels was observed with increasing culture time for both substrates. However, there were significant differences in the rate of the signal appearance between the regular and random patterns. The α-SMA stress fiber organization lagged behind the rate of YAP activation, as observed for the 75% regular versus random patterns. Looking at the 24 h point, a significant difference was observed in YAP activation between VICs on regular and random patterns. Interestingly, by 72 h, both activation levels plateaued to the same value (~60%). In contrast, α-SMA activation levels in VICs on the regular and random patterns were found to be at the same level at 24 h time point, after which the α-SMA activation levels on regular patterns increased faster, and a significant difference was observed between regular and random patterns at the 72 h time point. But interestingly, by 120 h, VICs seeded on the 75% regular and random

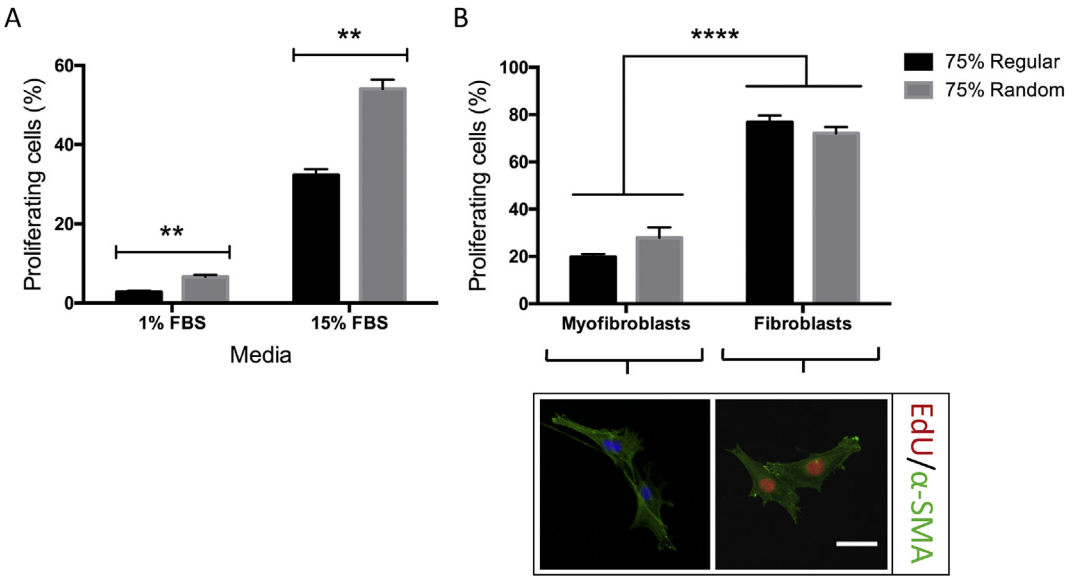

Fig. 5. Characterization of VICs proliferation on patterned substrates. A: The percentage of proliferating cells on 75% regular and random substrates in medium with 1% FBS or 15% FBS was quantified based on EdU staining. For both conditions there was found to be a significant higher percentage of proliferating cells on 75% random substrates than on 75% regular substrates. **: $p < 0.01$, based on one-way ANOVA analysis. $n = 3$ with triplicates, more than 200 cells were analyzed per sample. **(B)** The percentage of proliferating cells was quantified within the two subgroups of myofibroblasts and fibroblasts on 75% regular and random substrates. It was seen that the percentage of proliferating cells was higher in the subgroup of fibroblasts compared to the percentage of proliferating cells in the subgroup of myofibroblasts. This was seen for both 75% regular and random substrates. Representative images of both groups are shown, where green is α-SMA, red is EdU positive nucleus and blue is DAPI. Scale bar = 50 μm ****: $p < 0.0001$, based on one-way ANOVA. $n = 3$ with triplicates, more than 200 cells were analyzed per sample. (For interpretation of the references to colour in this figure legend, the reader is referred to the web version of this article.)

patterns reached the same final α-SMA activation level (~70%).

3.6. Focal adhesion size positively correlates with YAP activation

Focal adhesion, cytoskeleton tension and cell morphology have all been implicated in playing an important role in cell mechanotransduction processes which are regulated by YAP subcellular localization [26]. Based on the data in Fig. 7 at the 24 h time point, YAP activation was statistically different between VICs on regular and random patterns, and this difference further correlated with the α-SMA activation and proliferation differences at later time points. However, the cell morphology was the same between VICs on regular and random patterns at all time points, so it remained elusive what caused this YAP activation difference. We hypothesized that focal adhesions might lead to these differences in the YAP activation, so analysis of the focal adhesion size was conducted for VICs cultured on regular and random patterns. Focal adhesions were analyzed at the 24 h time point by immunostaining for paxillin, an important protein involved in focal adhesion complex formation [50]. A significant difference was observed between VICs on 75% regular versus random patterns; VICs on 75% regular patterns formed larger sized focal adhesions as shown by the representative images in Fig. 8A. More specifically, the average size of the VIC focal adhesions on the 75% regular pattern was 0.68 μm^2, which was statistically larger than the focal adhesions on the 75% random pattern with an average size of 0.56 μm^2 (Fig. 8B). Based on prior research [51], focal adhesion size has been reported to be an indicator of focal adhesion maturation, and might be important for mechanosensing in VICs. Our findings show that the size of the focal adhesions positively correlates with YAP activation at early time points, which also correlates with myofibroblast activation at later time points. Further studies are needed in order to figure out the mechanism of the positive correlation between focal adhesion maturation and YAP activation.

4. Discussion

Material properties, such as stiffness, topography and viscoelasticity have all been previously reported to influence cell fate [52,53]. Amongst these factors, elastic modulus has been widely studied in marrow-derived mesenchymal stem cells and shown to influence cell-matrix interactions, morphology and cell fate via mechanotransduction [54–56]. Previous studies show that cells sense the ECM through focal adhesions and cytoskeleton tension, and furthermore, matrix mechanics direct cell fate [57,58]. Here, our study demonstrates that VICs are capable of sensing matrix stiffness and make fate decisions independent of cell morphology and cytoskeleton organization (Fig. 2B and Supplemental Fig. 1). Specific to VICs, which respond to substrate modulus in both 2D and 3D [59,60], we have demonstrated that VICs are sensitive to relatively small changes in elastic moduli in 2D (Fig. 2), and additionally, their response depends on the matrix organization.

The results in this paper highlight a potentially important role of microenvironmental mechanical heterogeneity in affecting VICs and their activation from a quiescent fibroblast phenotype to a pathogenic myofibroblast phenotype. When events occur that lead to heterogeneous changes in the valve matrix organization and mechanics [61], for example myxomatous disease in heart valve, different cell behavior, like proliferation and activation into myofibroblasts, might be triggered. As shown by previous studies [5,61], more proliferation of fibroblasts and activation into myofibroblasts are expected during disease progression. The difference between this expectation and our *in vitro* experimental data might be attributed to two factors. Firstly, longer-term matrix disorganization and stiffening may play a role in the persistence of the myofibroblast population, as observed in the histopathology of diseased valves [2,62]. Therefore, it might be interesting to conduct longer *in vitro* studies of this progression. Such long-term studies would likely necessitate transitioning to a 3D cell-laden hydrogel, which will require developing improved methods to pattern and control

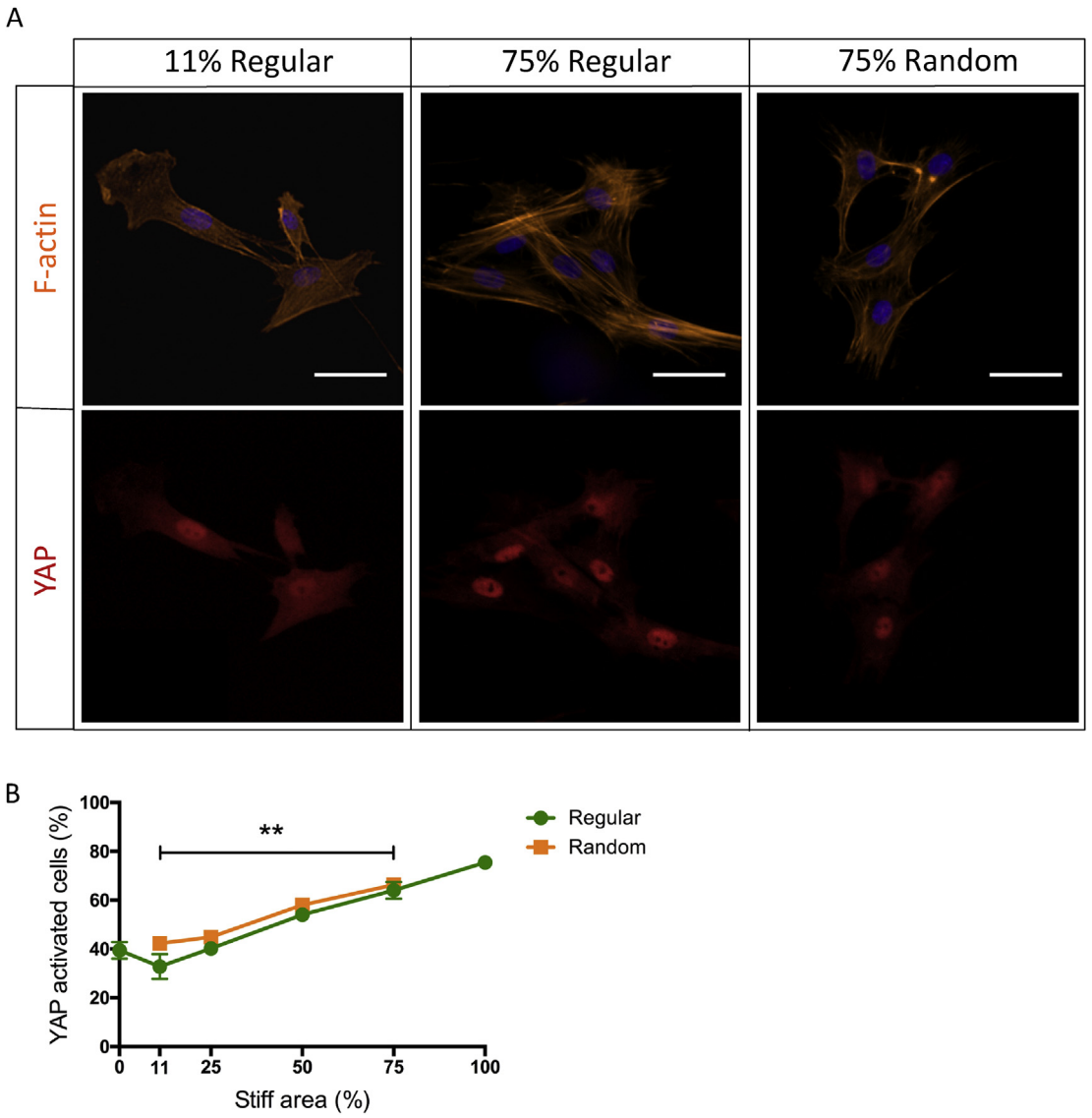

Fig. 6. Characterization of YAP activation on patterned substrates. A: Immunostaining of VICs on regular and random hydrogel surfaces after culturing for 72 h. F-actin fiber formation was seen on 11%, 75% regular and random substrates. YAP activation was seen on both the 75% regular and random substrates. DAPI (blue), F-actin (orange), YAP (red). Scale bars = 50 μm. **B**: The percentage of VICs with intracellular YAP activation was quantified based on the immunostaining. For both regular and random patterns YAP activation increases correspondingly to stiff percentages. There was found to be a significant increase in YAP activation from 11% regular to 75% regular (green line with circles) and 11% random to 75% random (orange line with squares). There was no difference observed between 75% regular and random. **: $p < 0.01$, based on one-way ANOVA. n = 3 with triplicates, more than 200 VICs were analyzed per sample. (For interpretation of the references to colour in this figure legend, the reader is referred to the web version of this article.)

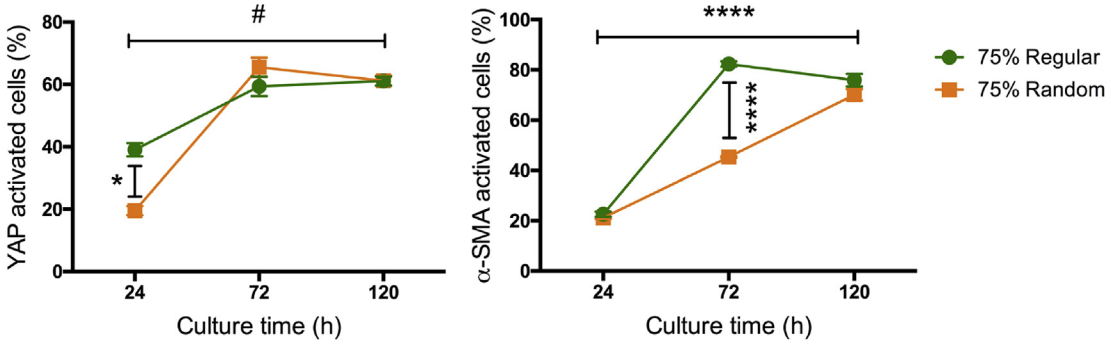

Fig. 7. Quantification of YAP and α-SMA activation at different time points. The percentages of α-SMA activated cells and YAP activated cells were analyzed at 24, 72 and 120 h. The percentage of α-SMA activated and YAP activated cells increased over time. Furthermore, there was found to be a significant different percentage of YAP activation on 75% regular and random substrates at time point 24 and a significant different percentage of α-SMA activation on 75% regular and random substrates at time point 72. ****: $p < 0.0001$ for both 75% regular and random substrates. #: $p < 0.01$ compared between 24 h and 120 h for 75% regular substrates, #: $p < 0.0001$ compared between 24 h and 120 h for 75% random substrates. *: $p < 0.05$. Based on one-way ANOVA analysis. n = 3, more than 200 cells were analyzed per sample.

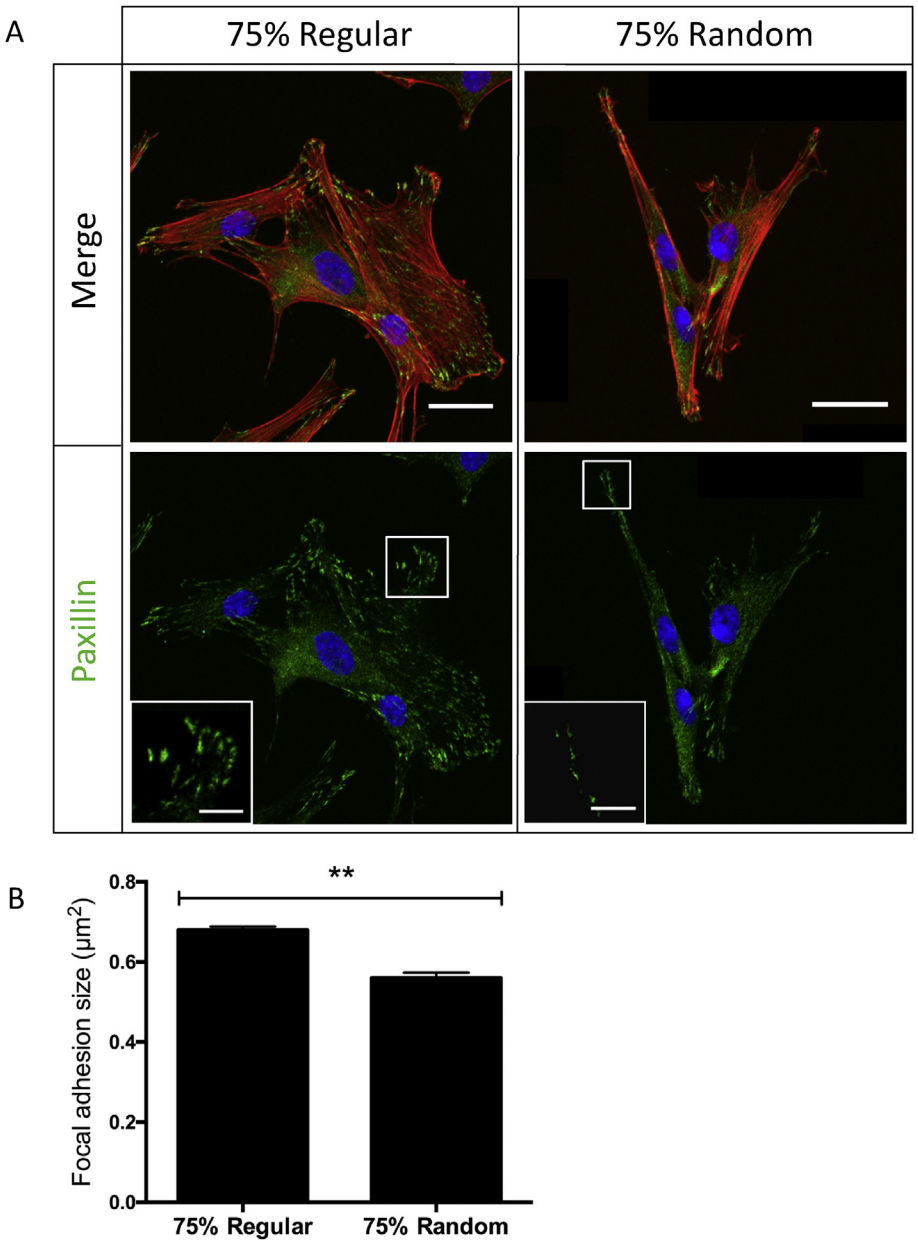

Fig. 8. Characterization of focal adhesion on patterned substrates. A: Focal adhesion formation was seen on 75% regular and 75% random after culturing for 24 h. It was observed that the focal adhesions from cells on 75% regular are larger in size than the focal adhesions formed on 75% random. DAPI (blue), F-actin (red), Paxillin (green). Scale bars = 30 μm. Inset image is magnification of outlined area, scale bar = 10 μm. **B**: Quantification of focal adhesion area was based on immunostaining. **: $p < 0.01$, based on non-parametric student t-test. n = 3 with triplicates, at least 20 cells were analyzed per sample.

matrix mechanics in 3D, along with complementary validation of image analysis methods in 3D. Secondly, the *in vivo* heterogeneous stiffness organization might be different from what VICs are sensing in our *in vitro* model. Therefore, quantification of the stiffness organization in valve tissue at different stages during disease progression, as well as in the different layers in the leaflet would be beneficial to further study the *in vivo* heterogeneous mechanical organization *in vitro*.

With respect to the short time response, the biological relevance of the reported results may more closely relate to VIC response to an injury, where heterogeneities exist in the matrix environment and likely influence local biomechanics and VIC mechanosensing. Here, VICs increase their population to facilitate collagen deposition and ECM remodeling, and then the stiffness of the valvular tissue increases with remodeling and time. Our *in vitro* model studies how increases in the stiffness and organization of the matrix can signal to VICs and activate them into myofibroblasts. This activation is known to increase VIC secretory properties [5], collagen deposition, and ECM stiffening [4], which if left unchecked, can lead to valve fibrosis [8]. More direct measurement of how VICs produce collagen on substrates with regular and random stiffness organization will provide insight to the contribution of collagen deposition to the development of valve fibrosis, as collagen production is independent of α-SMA activation during fibrosis in various organs [63].

The temporal analysis of YAP and α-SMA activation was

consistent with the literature that YAP subcellular localization is an early marker of mechanotransduction [43,64], and that matrix mechanical cues can further affect the conversion of VICs from fibroblasts to myofibroblasts, as demonstrated by α-SMA stress fiber formation. Future studies characterizing other molecular changes in the VICs (e.g., gene expression) during YAP nuclear localization may prove insightful, along with experiments to elucidate the mechanism by which YAP initiates α-SMA stress fiber formation, especially since our findings indicate that this process is independent of cell morphology and cytoskeleton organization.

Finally, our findings provide insight into how and why VICs are capable of sensing the heterogeneity of matrix mechanics and translate these extracellular signals into a cellular response. A better understanding of changes in the ECM composition and mechanical microenvironment during valve disease, such as fibrosis, along with cellular responses to this matrix signaling should prove useful in identifying pathways to target for therapeutic treatments.

Well-characterized biomaterial platforms, such as the one described in this paper, can provide an important link between the complexity of animal models of valve disease and highly controlled *in vitro* models for detailed hypothesis-testing about cellular responses and mechanisms. Here, we investigated hypotheses related to mechanosensing and matrix organization on VIC myofibroblast activation. We exploited a hydrogel with spatially tunable materials properties, but this same material also provides the opportunity to dynamically change the patterns and/or magnitude of the stiffness (e.g., soften the matrix) *in situ* [16,17] during *in vitro* VICs culturing. Future work will focus on culturing VICs in hydrogels and studying how they respond to changes in matrix properties in real time *in vitro*. The ability to conduct longer term experiments and study cyclical change in the matrix environment on VIC fibroblast-to-myofibroblast might be particularly insightful for understanding critical molecular changes that occur in VIC myofibroblasts when their activation persists, especially since many fibrotic tissues (e.g., heart, lung, kidney) have a high population of myofibroblasts.

5. Conclusion

In summary, we developed a photodegradable PEG based hydrogel system to spatially vary matrix elasticity and study the effect of matrix elasticity organization on VIC phenotype. Porcine VICs cultured on matrices with a higher percentage of stiff regions showed more α-SMA stress fibers and nuclear localized YAP, both of which are indicative of mechanical signaling and myofibroblast activation. When cultured on substrates with randomly organized matrix mechanics, VICs had smaller focal adhesions and delayed nuclear YAP localization at early time points compared to those cultured on substrates with regular pattern of the stiff regions. The difference in focal adhesion size and YAP activation positively correlated with α-SMA activation at later time points. Moreover, α-SMA activated VICs had lower proliferation rates compared to α-SMA deactivated VICs, which implies a potential biological mechanism that VICs sense a disorganization in ECM through spatially varying matrix stiffness, as often occurs during the beginning stages of wound healing and disease progression. This matrix-cellular signaling influences the VIC fibroblast-to-myofibroblast transition in a manner that may correlate to differences between healthy ECM remodeling (e.g., homeostasis) versus pathogenic fibrosis.

Acknowledgements

The authors would like to thank Andrea Gonzalez Rodriguez and Megan E. Schroeder for help with VIC isolation, Cierra J. Walker for help with qPCR, Ella A. Hushka and Brett A. Jeffrey for help with VICs culturing as well as Tova L. Christensen for discussion. The focal adhesion imaging work was performed at the BioFrontiers Institute Advanced Light Microscopy Core. Laser scanning confocal microscopy was performed on a Nikon A1R microscope acquired by the generous support of the NIST-CU Cooperative Agreement award number 70NANB15H226. The authors would also like to acknowledge the support of National Institutes of Health (Grants R01 RHL132353A and R21 AR067469) and the Howard Hughes Medical Institute (K.S.A). Specific commercial equipment, instruments, and materials that are identified in this report are listed in order to adequately describe the experimental procedure and are not intended to imply endorsement or recommendation by the National Institute of Standards and Technology (NIST).

Appendix A. Supplementary data

Supplementary data related to this article can be found at http://dx.doi.org/10.1016/j.biomaterials.2017.03.040.

References

[1] A.D. Durbin, A.I. Gotlieb, Advances towards understanding heart valve response to injury, Cardiovasc. Pathol. 11 (2) (2002) 69–77.
[2] A.C. Liu, V.R. Joag, A.I. Gotlieb, The emerging role of valve interstitial cell phenotypes in regulating heart valve pathobiology, Am. J. Pathol. 171 (5) (2007) 1407–1418.
[3] A.C. Liu, A.I. Gotlieb, Characterization of cell motility in single heart valve interstitial cells in vitro, Histol. Histopathol. 22 (2007) 873–882.
[4] E. Rabkin, M. Aikawa, J.R. Stone, Y. Fukumoto, P. Libby, F.J. Schoen, Activated interstitial myofibroblasts express catabolic enzymes and mediate matrix remodeling in myxomatous heart valves, Circulation 104 (21) (2001) 2525–2532.
[5] E. Rabkin-Aikawa, M. Farber, M. Aikawa, F.J. Schoen, Dynamic and reversible changes of interstitial cell phenotype during remodeling of cardiac valves, J. Heart Valve Dis. 13 (5) (2004) 841–847.
[6] R.B. Hinton, K.E. Yutzey, Heart valve structure and function in development and disease, Annu. Rev. Physiol. 73 (2011) 29.
[7] S. Sell, R.E. Scully, Aging changes in the aortic and mitral valves: histologic and histochemical studies, with observations on the pathogenesis of calcific aortic stenosis and calcification of the mitral annulus, Am. J. Pathol. 46 (3) (1965) 345.
[8] F. Liu, J.D. Mih, B.S. Shea, A.T. Kho, A.S. Sharif, A.M. Tager, D.J. Tschumperlin, Feedback amplification of fibrosis through matrix stiffening and COX-2 suppression, J. Cell Biol. 190 (4) (2010) 693–706.
[9] K. Wyss, C.Y. Yip, Z. Mirzaei, X. Jin, J.H. Chen, C.A. Simmons, The elastic properties of valve interstitial cells undergoing pathological differentiation, J. Biomech. 45 (5) (2012) 882–887.
[10] S.M. Levenson, E.F. Geever, L.V. Crowley, J.F. Oates III, C.W. Berard, H. Rosen, Healing of rat skin wounds, Ann. Surg. 161 (2) (1965) 293.
[11] A. Hervas, A. Ruiz-Sauri, E. Dios, M.J. Forteza, G. Minana, J. Nunez, …, F.J. Chorro, Inhomogeneity of collagen organization within the fibrotic scar after myocardial infarction: results in a swine model and in human samples, J. Anat. 228 (1) (2016) 47–58.
[12] S. Huang, H.Y.S. Huang, Biaxial stress relaxation of semilunar heart valve leaflets during simulated collagen catabolism: effects of collagenase concentration and equibiaxial strain state, Proc. Inst. Mech. Eng. Part H J. Eng. Med. 229 (10) (2015) 721–731.
[13] W.D. Merryman, I. Youn, H.D. Lukoff, P.M. Krueger, F. Guilak, R.A. Hopkins, …, S. Michael, Correlation between heart valve interstitial cell stiffness and transvalvular pressure: implications for collagen biosynthesis, Am. J. Physiol. Heart Circulat. Physiol. 59 (1) (2006) H224.
[14] A.C. Liu, A.I. Gotlieb, Transforming growth factor-β regulates in vitro heart valve repair by activated valve interstitial cells, Am. J. Pathol. 173 (5) (2008) 1275–1285.
[15] C. Yang, F.W. DelRio, H. Ma, A.R. Killaars, L.P. Basta, K.A. Kyburz, K.S. Anseth, Spatially patterned matrix elasticity directs stem cell fate, Proc. Natl. Acad. Sci. 113 (31) (2016) E4439–E4445.
[16] A.M. Kloxin, A.M. Kasko, C.N. Salinas, K.S. Anseth, Photodegradable hydrogels for dynamic tuning of physical and chemical properties, Science 324 (5923) (2009) 59–63.
[17] C. Yang, M.W. Tibbitt, L. Basta, K.S. Anseth, Mechanical memory and dosing influence stem cell fate, Nat. Mater. 13 (6) (2014) 645.
[18] M.A. Bowler, W.D. Merryman, In vitro models of aortic valve calcification: solidifying a system, Cardiovasc. Pathol. 24 (1) (2015) 1–10.
[19] M.H. Kural, K.L. Billiar, Mechanoregulation of valvular interstitial cell phenotype in the third dimension, Biomaterials 35 (4) (2014) 1128–1137.
[20] A.M. Kloxin, J.A. Benton, K.S. Anseth, In situ elasticity modulation with

dynamic substrates to direct cell phenotype, Biomaterials 31 (1) (2010) 1–8.
[21] A.M. Quinlan, K.L. Billiar, Investigating the role of substrate stiffness in the persistence of valvular interstitial cell activation, J. Biomed. Mater. Res. Part A 100 (9) (2012) 2474–2482.
[22] S. Dupont, Role of YAP/TAZ in cell-matrix adhesion-mediated signalling and mechanotransduction, Exp. Cell Res. 343 (1) (2016) 42–53.
[23] S. Dupont, L. Morsut, M. Aragona, E. Enzo, S. Giulitti, M. Cordenonsi, …, N. Elvassore, Role of YAP/TAZ in mechanotransduction, Nature 474 (7350) (2011) 179–183.
[24] Y. Cui, F.M. Hameed, B. Yang, K. Lee, C.Q. Pan, S. Park, M. Sheetz, Cyclic stretching of soft substrates induces spreading and growth, Nat. Commun. 6 (2015).
[25] S.R. Caliari, M. Perepelyuk, E.M. Soulas, G.Y. Lee, R.G. Wells, J.A. Burdick, Gradually softening hydrogels for modeling hepatic stellate cell behavior during fibrosis regression, Integr. Biol. 8 (6) (2016) 720–728.
[26] S.R. Caliari, M. Perepelyuk, B.D. Cosgrove, S.J. Tsai, G.Y. Lee, R.L. Mauck, …, J.A. Burdick, Stiffening hydrogels for investigating the dynamics of hepatic stellate cell mechanotransduction during myofibroblast activation, Sci. Rep. 6 (2016).
[27] F. Calvo, N. Ege, A. Grande-Garcia, S. Hooper, R.P. Jenkins, S.I. Chaudhry, …, E. Sahai, Mechanotransduction and YAP-dependent matrix remodelling is required for the generation and maintenance of cancer-associated fibroblasts, Nat. Cell Biol. 15 (6) (2013) 637–646.
[28] P.C. Hiemenz, T.P. Lodge, Polymer Chemistry, CRC press, 2007.
[29] J.L. Hutter, J. Bechhoefer, Calibration of atomic-force microscope tips, Rev. Sci. Instrum. 64 (7) (1993) 1868–1873.
[30] I.N. Sneddon, The relation between load and penetration in the axisymmetric Boussinesq problem for a punch of arbitrary profile, Int. J. Eng. Sci. 3 (1) (1965) 47–57.
[31] C.M. Johnson, M.N. Hanson, S.C. Helgeson, Porcine cardiac valvular subendothelial cells in culture: cell isolation and growth characteristics, J. Mol. Cell. Cardiol. 19 (12) (1987) 1185–1193.
[32] F. Zanella, J.B. Lorens, W. Link, High content screening: seeing is believing, Trends Biotechnol. 28 (5) (2010) 237–245.
[33] B. Duan, Z. Yin, L.H. Kang, R.L. Magin, J.T. Butcher, Active tissue stiffness modulation controls valve interstitial cell phenotype and osteogenic potential in 3D culture, Acta biomater. 36 (2016) 42–54.
[34] J.A. Benton, B.D. Fairbanks, K.S. Anseth, Characterization of valvular interstitial cell function in three dimensional matrix metalloproteinase degradable PEG hydrogels, Biomaterials 30 (34) (2009) 6593–6603.
[35] J.A. Benton, H.B. Kern, K.S. Anseth, Substrate properties influence calcification in valvular interstitial cell culture, J. heart valve Dis. 17 (6) (2008) 689.
[36] M.C. Cushing, J.T. Liao, M.P. Jaeggli, K.S. Anseth, Material-based regulation of the myofibroblast phenotype, Biomaterials 28 (23) (2007) 3378–3387.
[37] H. Wang, L.A. Leinwand, K.S. Anseth, Cardiac valve cells and their microenvironment-insights from in vitro studies, Nat. Rev. Cardiol. 11 (12) (2014) 715–727.
[38] R. McBeath, D.M. Pirone, C.M. Nelson, K. Bhadriraju, C.S. Chen, Cell shape, cytoskeletal tension, and RhoA regulate stem cell lineage commitment, Dev. Cell 6 (4) (2004) 483–495.
[39] A.J. Maniotis, C.S. Chen, D.E. Ingber, Demonstration of mechanical connections between integrins, cytoskeletal filaments, and nucleoplasm that stabilize nuclear structure, Proc. Natl. Acad. Sci. 94 (3) (1997) 849–854.
[40] C.H. Thomas, J.H. Collier, C.S. Sfeir, K.E. Healy, Engineering gene expression and protein synthesis by modulation of nuclear shape, Proc. Natl. Acad. Sci. 99 (4) (2002) 1972–1977.
[41] H. Lee, W.J. Adams, P.W. Alford, M.L. McCain, A.W. Feinberg, S.P. Sheehy, …, K.K. Parker, Cytoskeletal prestress regulates nuclear shape and stiffness in cardiac myocytes, Exp. Biol. Med. 240 (11) (2015) 1543–1554.
[42] K.N. Dahl, A.J. Ribeiro, J. Lammerding, Nuclear shape, mechanics, and mechanotransduction, Circulation Res. 102 (11) (2008) 1307–1318.
[43] H. Wang, M.W. Tibbitt, S.J. Langer, L.A. Leinwand, K.S. Anseth, Hydrogels preserve native phenotypes of valvular fibroblasts through an elasticity-regulated PI3K/AKT pathway, Proc. Natl. Acad. Sci. 110 (48) (2013) 19336–19341.
[44] H. Wang, S.M. Haeger, A.M. Kloxin, L.A. Leinwand, K.S. Anseth, Redirecting valvular myofibroblasts into dormant fibroblasts through light-mediated reduction in substrate modulus, PloS one 7 (7) (2012) e39969.
[45] M.C. Cushing, M.P. Jaeggli, K.S. Masters, L.A. Leinwand, K.S. Anseth, Serum deprivation improves seeding and repopulation of acellular matrices with valvular interstitial cells, J. Biomed. Mater. Res. Part A 75 (1) (2005) 232–241.
[46] R. Ross, J. Glomset, B. Kariya, L. Harker, A platelet-dependent serum factor that stimulates the proliferation of arterial smooth muscle cells in vitro, Proc. Natl. Acad. Sci. 71 (4) (1974) 1207–1210.
[47] M.B. Vaughan, T.D. Odejimi, T.L. Morris, D. Sawalha, C.L. Spencer, A new bioassay identifies proliferation ratios of fibroblasts and myofibroblasts, Cell Biol. Int. 38 (8) (2014) 981–986.
[48] T. Yamamoto, J. Varani, H.K. Soong, P.R. Lighter, Effects of 5-fluorouracil and mitomycin C on cultured rabbit subconjunctival fibroblasts, Ophthalmology 97 (9) (1990) 1204–1210.
[49] F. Liu, D. Lagares, K.M. Choi, L. Stopfer, A. Marinković, V. Vrbanac, …, I.O. Rosas, Mechanosignaling through YAP and TAZ drives fibroblast activation and fibrosis, Am. J. Physiol. Lung Cell. Mol. Physiol. 308 (4) (2015) L344–L357.
[50] E. Zamir, M. Katz, Y. Posen, N. Erez, K.M. Yamada, B.Z. Katz, …, B. Geiger, Dynamics and segregation of cell–matrix adhesions in cultured fibroblasts, Nat. Cell Biol. 2 (4) (2000) 191–196.
[51] J.M. Goffin, P. Pittet, G. Csucs, J.W. Lussi, J.J. Meister, B. Hinz, Focal adhesion size controls tension-dependent recruitment of α-smooth muscle actin to stress fibers, J. Cell Biol. 172 (2) (2006) 259–268.
[52] P.M. Taylor, P. Batten, N.J. Brand, P.S. Thomas, M.H. Yacoub, The cardiac valve interstitial cell, Int. J. Biochem. Cell Biol. 35 (2) (2003) 113–118.
[53] E.R. Mohler, F. Gannon, C. Reynolds, R. Zimmerman, M.G. Keane, F.S. Kaplan, Bone formation and inflammation in cardiac valves, Circulation 103 (11) (2001) 1522–1528.
[54] C. Fayet, M.P. Bendeck, A.I. Gotlieb, Cardiac valve interstitial cells secrete fibronectin and form fibrillar adhesions in response to injury, Cardiovasc. Pathol. 16 (4) (2007) 203–211.
[55] C.I. Fisher, J. Chen, W.D. Merryman, Calcific nodule morphogenesis by heart valve interstitial cells is strain dependent, Biomechanics Model. Mechanobiol. 12 (1) (2013) 5–17.
[56] D.S. Puperi, L.R. Balaoing, R.W. O'Connell, J.L. West, K.J. Grande-Allen, 3-Dimensional spatially organized PEG-based hydrogels for an aortic valve co-culture model, Biomaterials 67 (2015) 354–364.
[57] K.M. Mabry, R.L. Lawrence, K.S. Anseth, Dynamic stiffening of poly (ethylene glycol)-based hydrogels to direct valvular interstitial cell phenotype in a three-dimensional environment, Biomaterials 49 (2015) 47–56.
[58] J.S. Soares, J.A. Stella, W. Zhang, N.J. Amoroso, J.E. Mayer, W.R. Wagner, M.S. Sacks, Large strain stimulation promotes extracellular matrix production and stiffness in an elastomeric scaffold model, J. Mech. Behav. Biomed. Mater. 62 (2016) 619–635.
[59] N.M. Rajamannan, F.J. Evans, E. Aikawa, K.J. Grande-Allen, L.L. Demer, D.D. Heistad, …, F.J. Schoen, Calcific aortic valve disease: not simply a degenerative process a review and agenda for research from the national heart and lung and blood Institute aortic stenosis working GroupExecutive summary: calcific aortic valve Disease–2011 update, Circulation 124 (16) (2011) 1783–1791.
[60] B. Hinz, Formation and function of the myofibroblast during tissue repair, J. Investig. Dermatol. 127 (3) (2007) 526–537.
[61] E. Rabkin-Aikawa, J.E. Mayer Jr., F.J. Schoen, Heart valve regeneration, in: Regenerative Medicine II, Springer Berlin Heidelberg, 2005, pp. 141–179.
[62] C. Fayet, M.P. Bendeck, A.I. Gotlieb, Cardiac valve interstitial cells secrete fibronectin and form fibrillar adhesions in response to injury, Cardiovasc. Pathol. 16 (4) (2007) 203–211.
[63] K.H. Sun, Y. Chang, N.I. Reed, D. Sheppard, α-Smooth muscle actin is an inconsistent marker of fibroblasts responsible for force-dependent TGFβ activation or collagen production across multiple models of organ fibrosis, Am. J. Physiol. Lung Cell. Mol. Physiol. 310 (9) (2016) L824–L836.
[64] J.A. Benton, C.A. DeForest, V. Vivekanandan, K.S. Anseth, Photocrosslinking of gelatin macromers to synthesize porous hydrogels that promote valvular interstitial cell function, Tissue Eng. Part A 15 (11) (2009) 3221–3230.